IEEE Access
Multidisciplinary | Rapid Review | Open Access Journal

Received 22 January 2024, accepted 1 February 2024, date of publication 20 February 2024, date of current version 6 May 2024.

Digital Object Identifier 10.1109/ACCESS.2024.3368033

RESEARCH ARTICLE

Comprehensive Electro-Magnetic Protection Method of Radio Fuze for Electro-Magnetic Rail-Gun

RUIHU WEN[1,2] **AND PING LI**[1]

[1]School of Mechatronical Engineering, Beijing Institute of Technology, Beijing 100081, China
[2]Science and Technology on Electromechanical Dynamic Control Laboratory, Xi'an Institute of Electromechanical Information Technology, Xi'an 710065, China

Corresponding author: Ruihu Wen (15830273920@163.com)

ABSTRACT When the electro-magnetic rail-gun is fired, the transient strong magnetic field environment in the bore will produce induced current in the radio fuze circuit and affect the normal operation of the fuze. Therefore, reasonable shielding and protective measures need to be taken to ensure the reliable operation of the fuze control circuit. Based on Faraday's law of electro-magnetic induction, a comprehensive electro-magnetic protection method for radio fuze suitable for electro-magnetic rail-gun is proposed in this paper. This method utilizes a high permeability material shell for magnetic shielding to decrease the magnetic induction intensity of the fuze circuit. Additionally, the eddy current effect of high conductivity metal material is utilized to slow down the change rate of magnetic induction intensity of the fuze circuit. The circuit area of the fuze is minimized through reasonable circuit design, and the layout of the circuit board is optimized to reduce the dot multiplication of the circuit loop area vector and the magnetic field direction. Through the simulation analysis of the finite element model of radio fuze in strong magnetic field, the effectiveness of the above electro-magnetic protection method was proved. The research results of this paper can provide reference for the design of radio fuze of electro-magnetic rail-gun.

INDEX TERMS Electro-magnetic induction, electro-magnetic rail-gun, induced electromotive force, radio fuze.

I. INTRODUCTION

The electro-magnetic rail-gun is a novel launcher that utilizes the Lorentz force to accelerate a projectile to ultra-high speeds [1], [2], [3], [4]. By controlling the current, the ideal launch speed of the projectile can be achieved as the Lorentz force varies with the current. In the launching process, the armature needs to push the projectile to an ultra-high speed of km/s in a very short time, so it needs to apply extended pulse high current excitation to the armature through the guide rail. The large current applied instantaneously will produce a transient strong electro-magnetic field in the rail-gun bore [5], [6], [7], [8], [9], [10]. The transient electro-magnetic field in the launch process of the electro-magnetic rail-gun is calculated and analyzed by establishing the launch model and using calculation and simulation methods. This allows for the simulation of the electro-magnetic field distribution in the bore during the launching process of the electro-magnetic rail-gun.

At present, to get rid of the current situation of uncontrolled projectile of electro-magnetic gun and to give full play to its maximum damage efficiency, military powers have considered development of intelligent ammunition of electro-magnetic rail-gun [11], [12], [13], [14], [15]. As an important part of intelligent ammunition, fuze plays a role in the safety and initiation control of projectile. The detection and firing control circuit inside the fuze is affected by the transient strong magnetic field in the chamber during firing. Due to the induced electro-motive force generated by electro-magnetic induction, a large current is formed in the fuze circuit, resulting in the failure of electronic sensitive devices. If adequate shielding and protective measures are not taken, the fuse function would fail or even malfunction, causing damage to personnel and weaponry.

The associate editor coordinating the review of this manuscript and approving it for publication was Mohamed Kheir.

At present, most of the research focuses on the calculation of strong magnetic field in electro-magnetic rail-gun bore and the magnetic shielding of a single method [16], [17], [18], [19], [20], and there is little research on the comprehensive electro-magnetic protection method of radio fuze [21], [22], [23], [24]. The physical essence of the influence of a strong magnetic field environment on a radio detonator is that electro-magnetic induction produces an induced electromotive force. It generates a large current in the electronic circuit of the detonator, resulting in abnormal operation of the detonator. To solve this problem, based on Faraday's law of electro-magnetic induction, a comprehensive electro-magnetic protection method of radio fuze suitable for electro-magnetic rail-gun is pro-posed in this paper. Through the simulation analysis of the finite element model of radio fuze in strong magnetic field, the effectiveness of the above electro-magnetic protection method is proved.

Compared with other methods, the shell with magnetic shielding material can better resist the interference of strong magnetic field, and help to improve the anti-interference ability of the fuze. At the same time, the vortex effect of high conductivity is used to reduce the rate of magnetic induction intensity. This method helps to reduce the transient current in the circuit, reduce the influence of the electro-magnetic pulse on the fuze, and then improve the stability and reliability of the fuze. The contribution of this study lies in the use of comprehensive electro-magnetic protection methods, combining magnetic shielding, eddy current effects, and optimized circuit design. This makes the fuse more stable and reliable during the electro-magnetic rail-gun launch process, which helps to improve the safety and success rate of projectile launch.

II. ANALYSIS OF STRONG MAGNETIC FIELD ENVIRONMENT IN ELECTRO-MAGNETIC RAIL-GUN

A. COMPUTATIONAL MODEL

The magnetic orbit gun is a shooting weapon system that utilizes the principle of electro-magnetic force to accelerate shells to high speeds. This is achieved by passing a current through a magnetic field generated by a guide rail. The basic theory behind this system includes the principles of electro-magnetic force, guide rail design, and shell acceleration. The basic principle of an electro-magnetic orbital gun is to use Lorentz and magnetic forces to accelerate shells. A current passing through the rail creates a strong magnetic field. Inside the shell, a current interacts with the magnetic field of the rail to create a Lorentz force. The Lorentz force acts perpendicular to the current and magnetic field, propelling the shell forward and accelerating its movement. Additionally, the design of the guide rail is a crucial factor in the functioning of the electro-magnetic rail-gun. The guide rail should possess excellent electrical conductivity and high temperature resistance, typically utilizing highly conductive metals such as copper or aluminum. The design of the guide rail's shape and size should also consider the characteristics of the shell to ensure a steady passage and full acceleration. The electro-magnetic orbital gun's core process is the acceleration of shells. A shell carries a current and is subjected to a Lorentz force through the magnetic field of the guide rail, which accelerates its movement. To achieve high-speed firing, shell design must consider factors such as mass, shape, and current. Simultaneously, it is crucial to maintain good electrical contact between the shell and the guide rail to ensure smooth current flow. The working principle of the electro-magnetic rail-gun is shown in Figure 1. The two parallel guide rails carry a pulsed large current that generates a strong magnetic field between them. This magnetic field interacts with the current flowing through the armature, creating a powerful ampere force that propels the armature forward at high speed. The projectile is launched at ultra-high speed from the front end of the armature.

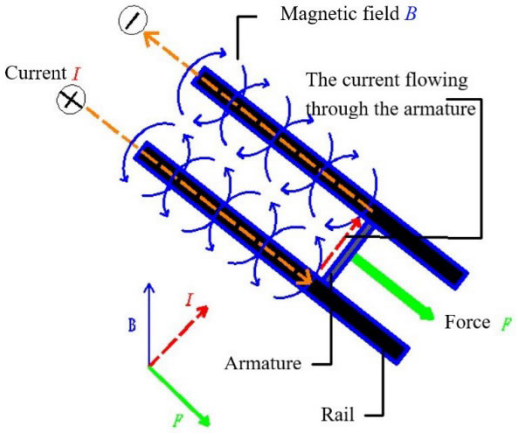

FIGURE 1. Schematic diagram of electro-magnetic rail-gun.

Figure 2 shows a three-dimensional transient electro-magnetic simulation model of an electro-magnetic rail-gun intelligent ammunition, including a radio fuze, established in Maxwell electro-magnetic simulation software. The guide rail, made of copper, is 20 mm thick, 140 mm high, and 3000 mm long. The armature is saddle-shaped and made of aluminum. The caliber of the shell is 90 mm, the length is 610 mm, and the material is steel.

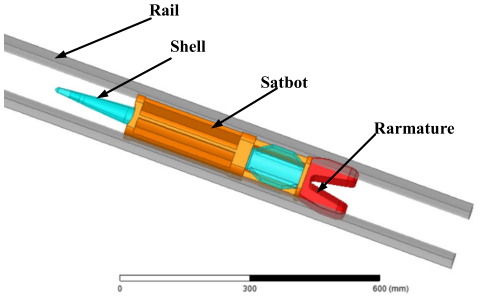

FIGURE 2. Electro-magnetic simulation model.

Figure 3 shows that the excitation current of the electro-magnetic rail-gun consists of multiple groups of double

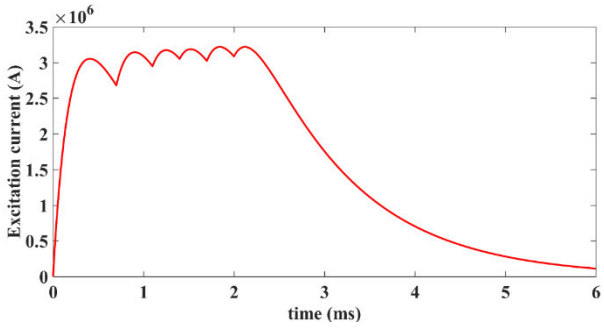

FIGURE 3. Excitation current.

exponential pulse currents. The maximum excitation current is 3.2 MA, with a pulse current rising edge time of 0.41 ms, a current peak duration of 1.74 ms, and a total duration of 6 ms.

In the three-dimensional transient electro-magnetic simulation model of the electro-magnetic rail-gun firing ammunition in Figure 2, using the current in Figure 3 as the excitation source, the spatio-temporal distribution response characteristics of the magnetic field inside the electro-magnetic rail-gun barrel can be simulated and calculated.

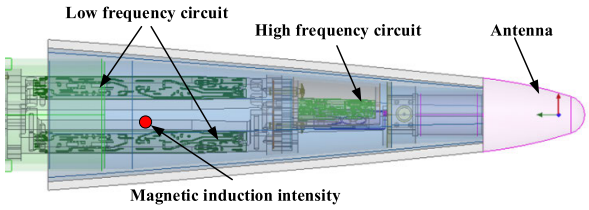

FIGURE 4. Schematic diagram of radio fuze of electro-magnetic rail-gun.

Figure 4 shows the structural diagram of low-frequency circuit, high-frequency circuit and antenna in radio fuze. The observation point of magnetic induction intensity in the fuze is 500 mm away from the armature. The simulation analysis of the spatio-temporal response characteristics of the magnetic induction intensity and induced electro-motive force inside the radio fuse verifies the correctness of the comprehensive electro-magnetic protection method for the electro-magnetic rail-gun radio fuze. Electro-magnetic simulation experiments mainly utilize the finite element method due to its efficiency in handling complex electro-magnetic field problems, including magnetic and electric fields as well as their mutual coupling. Meanwhile, simulations are conducted in the time domain. Time domain simulation can capture the transient behavior of electro-magnetic waves, which is crucial for understanding the dynamic changes in the magnetic induction intensity and induced electro-motive force inside the fuze. The simulation establishes specific boundary conditions. An open boundary is set outside the fuze to allow the propagation of electro-magnetic waves, while a perfect magnetic boundary is set inside the fuze to simulate its impact on the internal magnetic field.

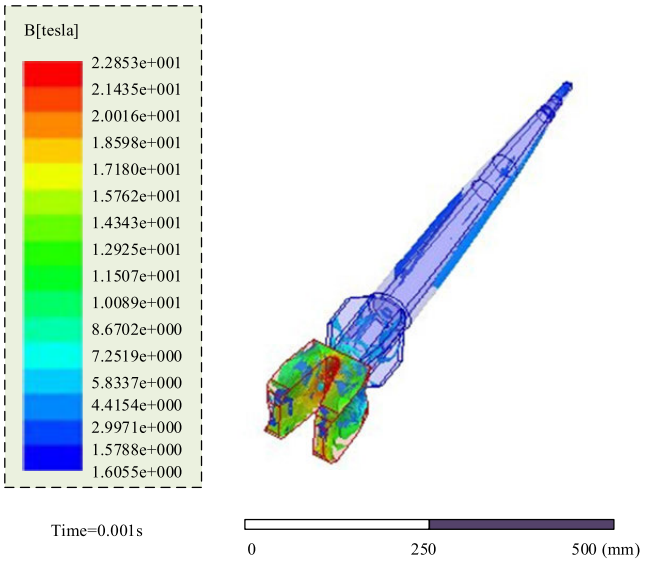

FIGURE 5. The distribution of magnetic field in different positions.

B. SIMULATION ANALYSIS

Figure 5 displays a cloud diagram of the magnetic field distribution at various positions of the armature and missile body. The figure illustrates that the magnetic induction intensity increases as the distance from the armature decreases. The maximum magnetic field intensity is 22.8 T at the armature position.

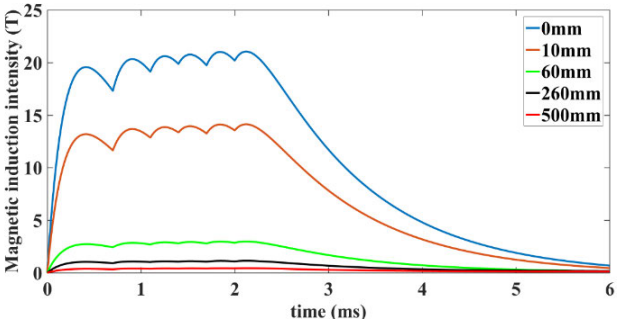

FIGURE 6. The curve of magnetic induction intensity with time at different distance from armature.

Figure 6 displays the curve of magnetic induction intensity over time at various distances from the armature, including 0 mm, 10 mm, 60 mm, 260 mm, and 500 mm. The simulation results indicate that the magnetic induction intensity decreases as the distance from the armature increases.

Table 1 lists the magnetic induction intensity at different positions away from the armature at different times. The table shows that maintaining the excitation current in the peak range results in a magnetic induction intensity of 20 T at the armature position, 13 T at a distance of 10 mm from the armature, 2.7 T at a distance of 60 mm from the armature, 1 T at a distance of 260 mm from the armature, and 0.4 T at a distance of 500 mm from the armature.

TABLE 1. Magnetic intensity at different positions of armature at different times.

Time (ms)	Distance from armature positon (mm)				
	0	10	60	260	500
0.1	10.7	7.21	1.48	0.56	0.2
0.4	19.55	13.17	2.72	1.03	0.37
2	20.2	13.54	2.85	1.09	0.41
3.5	7.53	5.01	1.09	0.46	0.21

III. RESEARCH ON COMPREHENSIVE ELECTRO-MAGNETIC PROTECTION METHOD OF RADIO FUZE IN STRONG MAGNETIC FIELD ENVIRONMENT

During the launching process of the electro-magnetic railgun, the transient strong magnetic field shown in Figure 6 will be generated in the chamber. Due to electro-magnetic induction, strong electromotive force will be generated, and then large current will be generated in the electronic circuit of the fuze. In Figure 7, the induced current in the electronic circuit will make the fuze circuit work abnormally or even burn the sensitive electronic components in the circuit.

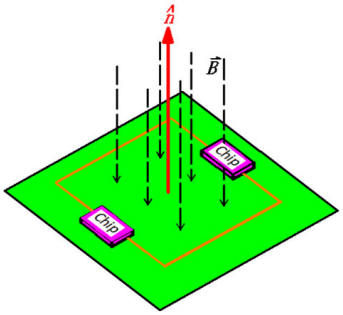

FIGURE 7. Schematic diagram of electro-magnetic induction.

According to Faraday's law of electro-magnetic induction, the induced electromotive force of fuze electronic circuit is:

$$V = -\frac{\partial \Phi}{\partial t} = -\int\int_s \frac{\partial \vec{B}}{\partial t} \cdot \vec{dS} \tag{1}$$

In Formula (1), V is the induced electromotive force. Φ is the magnetic flux passing through the electronic circuit. B is magnetic induction intensity. $\vec{S}$ is the loop area.

This paper proposes a comprehensive electro-magnetic protection method for radio fuze based on Faraday's law of electro-magnetic induction. The method includes reducing the magnetic induction intensity, the magnetic field change rate, the loop area, and the dot multiplication of the loop area vector and magnetic field direction.

A. REDUCE MAGNETIC INDUCTION

Reducing magnetic induction intensity is one of the important measures to protect radio fuses from electromagnetic interference. Choosing materials with high magnetic permeability to make magnetic shielding shells can effectively reduce magnetic induction. Materials with high magnetic permeability can absorb and disperse magnetic fields, thereby reducing the impact of magnetic induction on fuses. Common high permeability materials include iron, nickel alloys, and iron nickel alloys. Meanwhile, by increasing the thickness of the shielding layer, it is possible to better block the penetration of the magnetic field and reduce the transmission of magnetic induction intensity. In addition, by designing a reasonable magnetic shielding structure, the magnetic shielding effect can be further optimized. Figure 8 shows a simple cross-sectional view of magnetic shielding with high permeability materials, and the red part is the magnetic shielding shell. The figure shows that the magnetic material has a much greater magnetic permeability than the air inside the cavity. This means that the magnetic resistance of the air is greater than that of the magnetic material. As a result, most of the flux of the external magnetic field passes through the magnetic material, while less flux enters the cavity, achieving magnetic field shielding.

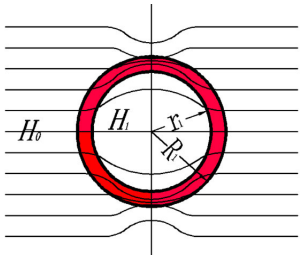

FIGURE 8. Magnetic shielding diagram.

According to the estimation formula of magnetic shielding effectiveness of cylindrical shell, Formula (2) is obtained.

$$H_1 = \frac{4\mu_r \cdot R_1^2 \cdot H_0}{R_1^2 (\mu_r + 1)^2 - r_1^2 (\mu_r - 1)^2} \tag{2}$$

In Formula (2), H_0 is the magnetic field force in the air domain outside the magnetic shielding. H_1 is the magnetic field strength in the cavity after the magnetic shielding. μ_r is the relative permeability of the shielding shell. R_1 is the outer diameter of the shielding shell, and r_1 is the inner diameter of the shielding shell.

Formula (2) shows that the shielding efficiency of the magnetic conductive material is directly proportional to its relative permeability. Increasing the thickness of the shielding shell can also enhance the shielding effect.

Based on the analysis above and the structural characteristics of the radio fuze shown in Figure 4, the simulation model was used to set and simulate the parameters of the material and thickness of the fuze shielding shell.

Figure 9 shows the comparison of magnetic shielding effectiveness of materials among different permeability (thickness 2 mm). To avoid overfitting the data, 100 sets of magnetic induction intensity data from the observation points were collected and divided into three groups: a training set (70% of the data), a validation set (20% of the data), and a test set (the remaining 10%). The figure shows that the

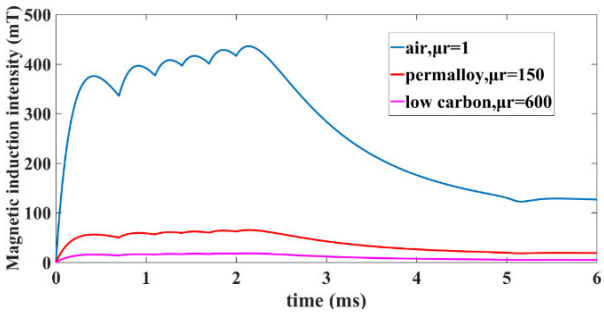

FIGURE 9. The comparison of magnetic shielding effectiveness of materials with different permeability.

maximum magnetic induction intensity at the observation point 500 mm away from the armature is 430 mT before shielding. After permalloy shielding, the maximum magnetic induction intensity decreases to 65 mT (shielding efficiency is 18.8 dB), and after low carbon steel shielding, it decreases to 18 mT (shielding efficiency is 31.7 dB).

Figure 10 shows the variation curve of magnetic induction intensity with time at the observation point 500 mm away from the armature when low carbon steel is used as the shielding material and the cavity thickness is 1 mm, 2 mm, 3 mm, 4 mm and 5 mm respectively. The simulation results show that the thicker the shield, the smaller the magnetic induction intensity inside the cavity.

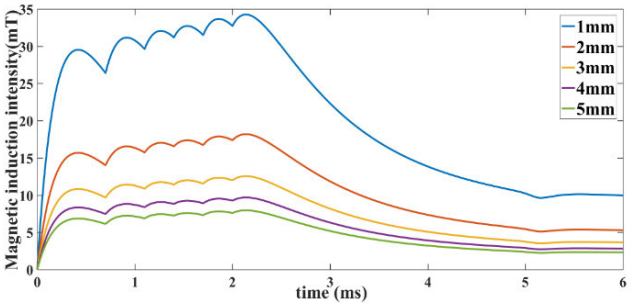

FIGURE 10. Comparison of magnetic shielding effectiveness of different thickness.

Table 2 lists the magnetic shielding effectiveness of low carbon steel with different thickness. When the thickness is 1mm, the peak value of magnetic induction intensity is 34.2 mT (shielding efficiency is 25.3 dB). When the thickness is 2 mm, the peak value of magnetic induction intensity is 18.18 mT (shielding efficiency 31.7 dB). When the thickness is 3 mm, the peak value of magnetic induction intensity is 12.54 mT (shielding efficiency is 35.3 dB). When the thickness is 4 mm, the peak value of magnetic induction intensity is 9.65 mT (shielding efficiency is 37.9 dB). When the thickness is 5 mm, the peak value of magnetic induction intensity is 7.91 mT (shielding efficiency is 39.9 dB).

TABLE 2. Shielding effectiveness of low carbon steel with different thickness.

Thickness of shielding layer (mm)	1	2	3	4	5
Peak value of magnetic induction intensity (mT)	34.2	18.18	12.54	9.65	7.91
Magnetic shielding efficiency (dB)	25.3	31.7	35.3	37.9	39.9

In order to more intuitively understand the relationship of the shield thickness and the magnetic induction intensity, and to analyze the ability of the shield to block the magnetic field in depth, the study further draws the correlation linear function. Figures 11 and 12 demonstrate the linear relationship between thickness and peak magnetic induction intensity. The simulation results indicate that the use of high permeability materials can significantly reduce the magnetic field intensity inside the shield.

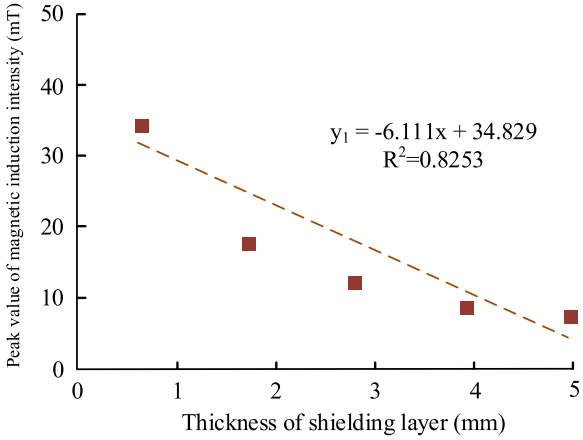

FIGURE 11. Linear relationship between different shielding layer thicknesses and peak value of magnetic induction intensity.

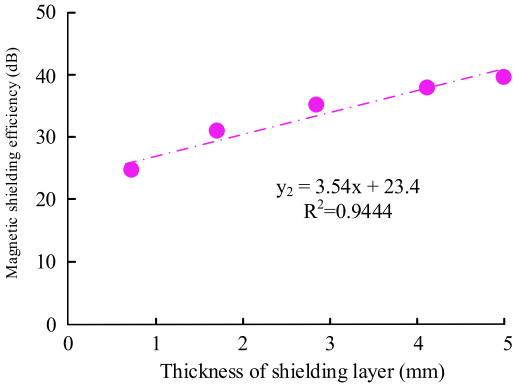

FIGURE 12. Linear relationship between different shielding layer thicknesses and magnetic shielding efficiency.

B. REDUCE THE CHANGE RATE OF MAGNETIC INDUCTION INTENSITY

When the external magnetic field changes, the metal shell will produce induced current. The magnetic field formed by induced current resists the change of external magnetic

field and slows down the change rate of magnetic field. The greater the conductivity, the better the mitigation effect of the change of external magnetic induction intensity. Based on this principle, high conductivity materials are used to electrically shield the external transient magnetic field, so as to reduce the change rate of magnetic induction intensity in the fuze.

Aluminum (σ =3.53 × 10^7S/m) and copper (σ =5.8 × 10^7S/m) are used to shield the external magnetic field respectively. Figure 13 shows the curve of magnetic induction intensity with time at a distance of 500 mm from the armature. The change rate of magnetic induction intensity inside the fuze cavity will be significantly slowed down after shielding with high conductivity materials.

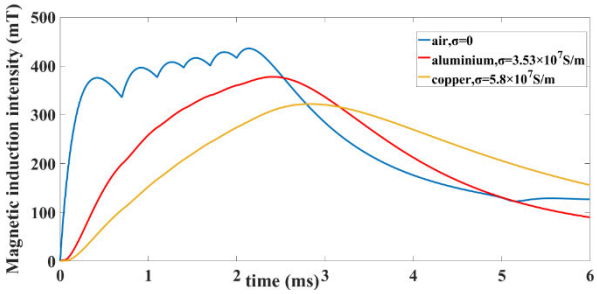

FIGURE 13. Change curve of magnetic induction intensity with time after shielding with different conductivity materials.

In Figure 14, without shielding, a transient strong magnetic field is generated at the rising edge of the pulse current and the connection time of the pulse current, and the change rate of magnetic induction intensity can reach 26.37. After shielding the fuze circuit with high conductivity materials such as aluminum and copper, the rate of change in magnetic induction intensity within the shielding cavity can be reduced to 3.87 and 1.98, respectively.

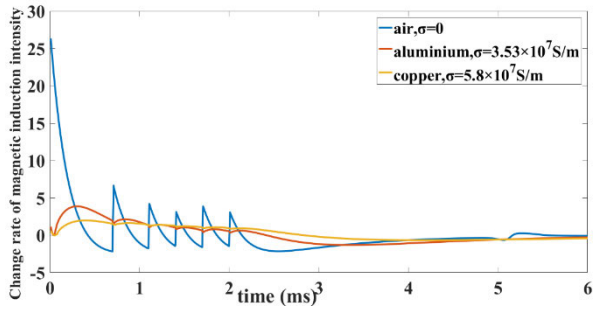

FIGURE 14. Change rate of magnetic induction intensity after shielding with different conductivity materials.

The simulation results show that the change rate of external magnetic field can be greatly reduced by using high conductivity materials.

C. REDUCE CIRCUIT LOOP AREA

Reducing the area of circuit loops is also one of the effective methods for electromagnetic protection. When designing circuits, it is possible to minimize the size of the circuit board and minimize the length of circuit wiring. This can reduce the loop area of the circuit and reduce the magnetic field interference it is subjected to. At the same time, it is necessary to arrange the circuit components reasonably, try to make the circuit wiring linear as much as possible, and reduce the bending and crossing of the circuit wiring. In Figure 15, when designing the fuze circuit, the area of the fuze circuit should be reduced as much as possible to reduce the magnetic flux passing through the fuze circuit and achieve the effect of reducing the induced electromotive force of the fuze circuit.

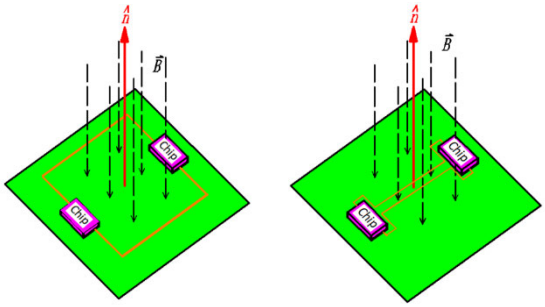

FIGURE 15. Schematic diagram of magnetic flux passing through the electronic circuit of fuze.

Formula (1) of Faraday's law of electro-magnetic induction can be used to calculate the induced electromotive force of the fuze circuit for different loop areas. Figure 16 illustrates the effect of loop areas on the induced electromotive force at a distance of 500 mm from the armature in the air domain. When the loop area is 5 mm^2, 20 mm^2 and 50 mm^2, the corresponding maximum induced electro-motive force is 0.13 mV, 0.52 mV and 1.32 mV, respectively.

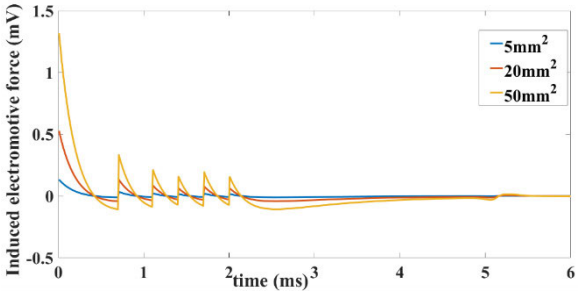

FIGURE 16. Influence of loop area on induced electro-motive force.

The calculation results show that the induced electro-motive force of fuze circuit can be effectively reduced by reducing the fuze loop area.

D. REDUCE THE DOT MULTIPLICATION OF LOOP AREA VECTOR AND MAGNETIC FIELD DIRECTION

In electromagnetic protection, reducing the dot product of loop area vector and magnetic field direction can help reduce the magnetic induction intensity on the circuit. When designing a circuit, the position of circuit components can be

adjusted reasonably to make the loop area of the circuit perpendicular or close to perpendicular to the direction of the magnetic field. Meanwhile, during the wiring process, it is advisable to avoid the direction of the circuit running parallel to the direction of the magnetic field as much as possible. Through this method, the dot product between the loop area vector and the magnetic field direction will decrease, thereby reducing the magnetic induction intensity experienced by the circuit. In Figure 17, the included angle between the circuit board and the magnetic field direction should be reduced as much as possible when the circuit board of electro-magnetic rail-gun fuze is arranged. To reduce the induced electromotive force of the fuze circuit, the dot multiplication value between the circuit area vector and the magnetic field direction is decreased.

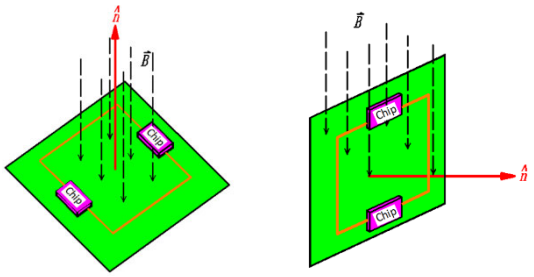

FIGURE 17. Schematic diagram of angle between circuit and magnetic field.

Formula (2) of Faraday's law of electro-magnetic induction can be used to calculate the induced electromotive force at different angles between the fuze circuit and the direction of the magnetic field. Figure 18 shows the influence of the action direction of the electronic circuit and the magnetic field direction on the induced electro-motive force when the air domain is 500 mm away from the armature and the fuze circuit area is 50 mm^2. When the included angle between the circuit and the magnetic field direction is 20°, 50° and 90°, the corresponding maximum induced electro-motive force is 0.45 mV, 1.01 mV and 1.32 mV.

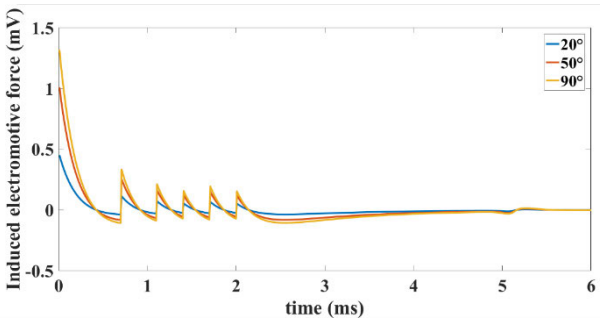

FIGURE 18. The influence of the angle between the electronic circuit and the magnetic field on the induced electro-motive force.

The calculation results show that reducing the angle between the circuit board and the magnetic field direction can effectively reduce the induced electro-motive force of the fuze circuit. The effect is the best when the circuit board is parallel to the magnetic line of force.

IV. CONCLUSION

This paper proposed a comprehensive electro-magnetic protection method for radio fuze suitable for electro-magnetic rail-gun based on Faraday's law of electro-magnetic induction. The method reduced the influence of the transient strong magnetic field in the bore on the radio fuze during electro-magnetic rail-gun launch, ensuring the normal and reliable operation of the fuze. The conclusions are as follows:

1) High permeability metal material is used for magnetic shielding to reduce the peak value of magnetic induction intensity B in radio fuze.

2) The eddy current effect of high conductivity material is used to reduce the change rate of magnetic induction intensity B in fuze.

3) The circuit design should minimize the circuit loop area to reduce the magnetic flux passing through the loop.

4) The angle between the circuit board and the magnetic field direction should be reduced as much as possible, so as to reduce the dot multiplication of the circuit area vector and the magnetic field direction.

REFERENCES

[1] D. Ceylan, M. Karagöz, Y. Çevik, B. Yildirim, H. Polat, and O. Keysan, "Simulations and experiments of EMFY-1 electromagnetic launcher," *IEEE Trans. Plasma Sci.*, vol. 47, no. 7, pp. 3336–3343, Jul. 2019.

[2] I. R. McNab, S. Fish, and F. Stefani, "Parameters for an electromagnetic naval railgun," *IEEE Trans. Mag.*, vol. 37, no. 1, pp. 223–228, Jan. 2001.

[3] J. Gallant, E. Vanderbeke, F. Alouahabi, and M. Schneider, "Design considerations for an electromagnetic railgun to be used against anti-ship missiles," *IEEE Trans. Plasma Sci.*, vol. 41, no. 10, pp. 2800–2804, Oct. 2013.

[4] S. Hundertmark and O. Liebfride, "Power supply options for a naval railgun," *IEEE Trans. Plasma Sci.*, vol. 46, no. 10, pp. 3599–3605, Oct. 2018.

[5] T. Stankevic, M. Schneider, and S. Balevicius, "Magnetic diffusion inside the rails of an electromagnetic launcher: Experimental and numerical studies," *IEEE Trans. Plasma Sci.*, vol. 41, no. 10, pp. 2790–2795, Oct. 2013.

[6] L. Gharib and A. Keshtkar, "Electromagnetic interference of railgun and its effect on surrounding electronics," *IEEE Trans. Plasma Sci.*, vol. 47, no. 8, pp. 4196–4202, Aug. 2019.

[7] W. G. Soper, "Electromagnetic field near rail guns," *IEEE Trans. Antennas Propag.*, vol. 37, no. 1, pp. 128–131, 1989.

[8] Q. Yin, H. Zhang, and H. Li, "Analysis of in-bore magnetic and electric fields in electromagnetic railgun under dynamic condition," *Acta Armamentarii*, vol. 38, no. 6, pp. 1059–1066, 2017.

[9] Y. Lou and B. Li, "Methods for reducing the loss caused by the eddy current in electromagnetic railgun shielding," *High Voltage Eng.*, vol. 42, no. 6, pp. 1935–1941, 2016.

[10] J. Li, "Linear current density and bore pressure of electromagnetic railgun," *High Voltage Eng.*, vol. 40, no. 4, pp. 1104–1109, 2014.

[11] J. Li, P. Yan, and W. Yan, "Electromagnetic gun technology and its development," *High Voltage Eng.*, vol. 40, no. 4, pp. 1052–1064, 2014.

[12] W. Ma, J. Lu, and X. Li, "Electromagnetic launch hypervelocity integrated projectile," *J. Nat. Univ. Tech.*, vol. 41, no. 4, pp. 1–10, 2019.

[13] A. Musolino, M. Raugi, R. Rizzo, and A. Tellini, "The multi-stage rail-gun," *IEEE Trans. Mag.*, vol. 37, no. 1, pp. 445–449, Jan. 2001.

[14] W. Xu, W. Yuan, Y. Che, R. Fu, J. Wang, D. Zhang, and P. Yan, "Velocity precision analysis with the small caliber electromagnetic launch," *IEEE Trans. Plasma Sci.*, vol. 45, no. 7, pp. 1394–1398, Jul. 2017.
[15] S. Hundertmark and D. Lancelle, "A scenario for a future European shipboard railgun," *IEEE Trans. Plasma Sci.*, vol. 43, no. 5, pp. 1194–1197, May 2015.
[16] A. Keshtkar, Z. Jafari Khorrami, and L. Gharib, "Comparison of inductance gradient and electromagnetic force in two types of railguns with two projectiles by finite-element method," *IEEE Trans. Plasma Sci.*, vol. 45, no. 8, pp. 2387–2392, Aug. 2017.
[17] R. Cao and X. Xu, "Analysis of the velocity and current measurement method based on B-dot probes for the rail gun," *IEEE Trans. Plasma Sci.*, vol. 45, no. 6, pp. 981–989, Jun. 2017.
[18] C. Li, L. Chen, Z. Wang, J. Ruan, P. Wu, J. He, and S. Xia, "Influence of armature movement velocity on the magnetic field distribution and current density distribution in railgun," *IEEE Trans. Plasma Sci.*, vol. 48, no. 6, pp. 2308–2315, Jun. 2020.
[19] Q. Lin and B. Li, "Measurement and numerical simulation of transient electromagnetic field in railgun," *Acta Armamentarii*, vol. 37, no. 10, pp. 1787–1794, 2016.
[20] F. Li, "Research on the shielding and utilization of electro-magnetic railgun's high magnetic field environment," M.S. thesis, Nanjing Univ. Sci. Technol., Nanjing, China, 2017.
[21] H.-B. Xie, H.-Y. Yang, J. Yu, M.-Y. Gao, J.-D. Shou, Y.-T. Fang, J.-B. Liu, and H.-T. Wang, "Research progress on advanced rail materials for electromagnetic railgun technology," *Defence Technol.*, vol. 17, no. 2, pp. 429–439, Apr. 2021.
[22] S. R. N. Praneeth, B. Singh, and J. P. Khatait, "Study on effect of rail filet radius in electromagnetic railgun," *IEEE Trans. Plasma Sci.*, vol. 49, no. 9, pp. 2997–3002, Sep. 2021.
[23] B. Zhu, J. Lu, X. Zhang, T. Ma, and Y. Dai, "A novel hybrid energy storage system for large shipborne electromagnetic railgun," *IEEE Trans. Plasma Sci.*, vol. 49, no. 8, pp. 2420–2427, Aug. 2021.
[24] K. Yu, H. Zhu, X. Xie, H. Duan, J. Ding, C. Sun, and Z. Bao, "Loss analysis of air-core pulsed alternator driving an ideal electromagnetic railgun," *IEEE Trans. Transport. Electrific.*, vol. 7, no. 3, pp. 1589–1599, Sep. 2021.

RUIHU WEN was born in Shanxi, China, in 1986. He received the B.S. degree in information and communication engineering from the University of Electronic Science and Technology of China, Chengdu, China, in 2008, and the M.S. degree in information and communication engineering from the Ordance Science Institute of China, Beijing, China, in 2011. He is currently pursuing the Ph.D. degree in armament science and technology with Beijing Institute of Technology, Beijing.

He is also an Associate Professor. His current research interests include pulsed power and electromagnetic launching techniques. He has published five relevant academic articles.

PING LI was born in Hebei, China, in 1966. She received the B.S. degree in machinery manufacturing process and equipment from Dalian Railway Institute, Dalian, China, in 1985, the M.S. degree in machinery manufacturing from Dalian University of Technology, Dalian, in 1987, and the Ph.D. degree in fuze technology from Beijing Institute of Technology, Beijing, China, in 1995.

She is currently a Professor with the School of Mechatronical Engineering, Beijing Institute of Technology. Her current research interests include intelligent detection and electromagnetic launching techniques. She has published more than 30 articles and four monographs.

Dr. Li served as the Vice Chairman of the Ammunition Safety Technical Committee of the Chinese Aerospace Society, a member of the Fuze Professional Committee of the Chinese Society of Ordnance Technology, and a member of the Special Equipment Committee of the Chinese Aerospace Society.